https://doi.org/10.46861/bmp.32.177 PŮVODNÍ PRÁCE/ORIGINAL PAPER

Polytypism of cronstedtite from two localities in Mexico

Jiří Hybler[1)#], Martin Števko[2,3)*], Zdeněk Dolníček[3)] and Jiří Sejkora[3)]

[1)] *Institute of Physics, Czech Academy of Sciences, Na Slovance 2, 182 21 Praha 8, Czech Republic; #died 25. 7. 2024*
[2)] *Earth Science Institute, v.v.i., Slovak Academy of Sciences, Dúbravská cesta 9, 840 05 Bratislava, Slovak Republic; *e-mail: martin.stevko@savba.sk*
[3)] *Department of Mineralogy and Petrology, National Museum, Cirkusová 1740, 193 00 Praha 9, Czech Republic*

Hybler J, Števko M, Dolníček Z, Sejkora J (2024) Polytypism of cronstedtite from two localities in Mexico. Bull Mineral Petrolog 32(2): 177-186 ISSN 2570-7337

Abstract

Cronstedtite from two Mexican localities: 1) San Antonio mine, 9th level, East camp, Santa Eulalia mining district, Aquiles Serdán Municipality, Chihuahua, Mexico (MSA in the following), 2) Francisco I. Madero Mine, Noria de los Gringos, Zacatecas, Mexico (FIM in the following), were studied by single-crystal X-ray diffraction using the four-circle diffractometer with area detector. The reciprocal space (RS) sections were generated by the diffractometer software in order to determine OD subfamilies (Bailey's groups) A, B, C, D, and particular polytypes. In the samples from MSA the polytype 3*T* (Subfamily A) is the most frequent. Some crystals are affected by twinning by reticular merohedry with the 180° rotation as twinning operation (obverse-reverse twinning). The $2H_2$ polytype (subfamily D) occurs rarely. In the FIM sample, the $2H_1$ + $2H_2$ allotwins (subfamily D) are most frequent. In one sample, the rare $6T_1$ polytype (subfamily D) was detected. The 3*T* polytype is rare. The electron probe microanalysis showed broad similarites in composition of the studied cronstedtites, characterized by common lack of any substitutes except of low S (up to 0.02 *apfu*; at both sites), and Cl (up to 0.01 *apfu*, at FIM only).

Keywords: *cronstedtite, 1:1 layer silicate, polytypism, twinning, Mexico*

Received 3. 7. 2024; accepted 9. 12. 2024

Introduction

Mineral cronstedtite, a 1:1 sheet silicate of kaolinite-serpentine group, with the general formula $(Fe^{2+}_{3-x}Fe^{3+}_{x})(Si_{2-x}Fe^{3+}_{x})O_5(OH)_4$, (where $0 < x < 0.85$), attracts attention from various points of view in last years. It was first described by Steinmann (1820, 1821) from the Vojtěch Mine in Příbram (now Czech Republic) and was named in honour of the Swedish chemist and mineralogist Axel Fredrik Cronstedt (23 December 1722 - 19 August 1765). Vrba (1886) described cronstedtite from Rejské Lode in Kaňk, near Kutná Hora (formerly known also as Kuttenberg, now Czech Republic).

Frondel (1962), Steadman and Nuttall (1963, 1964), Steadman (1964), and later Bailey (1969, 1988) studied cronstedtite by the single-crystal X-ray diffraction and recognized it as a T-O or 1:1 trioctahedral phyllosilicate of the serpentine-kaolinite group forming various polytypes.

Several detailed studies of polytypism of natural terrestrial cronstedtite from various localities were done recently: Pohled (Hybler et al. 2016), Chyňava (Hybler and Sejkora, 2017), Litošice (Hybler et al. 2021a) in the Czech Republic; Nižná Slaná, Slovakia (Hybler et al. 2017); Nagybörzsöny, Hungary (Hybler et al. 2020); and Ouedi Beht, El Hammam, Morocco (Hybler et al. 2021b).

Moreover, micrometer-sized synthetic crystals of cronstedtite were repeatedly prepared by Pignatelli et al. (2013, 2020) by the iron-clay or iron-quartz reactions at 60 - 90 °C and studied by electron diffraction by Hybler et al. (2018).

Cronstedtite occurs also in meteorites - CM chondrites, and Martian meteorites (Zega et al. 2003; Pignatelli et al. 2018; Garvie 2021). The presence of cronstedtite or serpentines with composition close to cronstedtite is assumed on the surface of the dwarf planet Ceres and Saturn's moon Enceladus (Zolotov, Mironenko 2013; Zolotov 2014; Roche et al. 2023).

The aim of this study is to describe polytypes of cronstedtite from two localities in Mexico.

Localities

The San Antonio mine is located approximately 30 km east of the Chihuahua city, Aquiles Serdán Municipality, Chihuahua State, Mexico (Fig. 1). GPS coordinates of the mine are: 28°36'12.6"N 105°49'00.4"W. The San Antonio mine is the principal mine of the East Camp, which is part of the famous Santa Eulalia mining district, a large intrusion-related carbonate replacement Pb-Zn-Ag deposit hosted by the Cretaceous limestone. The ore mineralization at the East Camp is characterized by bilaterally symmetrically zoned, intrusion-cored epidote-chlorite and sphalerite rich garnet-hedenbergite skarns with peripheral manto bodies of massive sulphides, containing mainly pyrrhotite, sphalerite, galena, arsenopyrite and pyrite (Megaw et al. 1988; Megaw 2018). Sample with cronstedtite (MSA in the following) was collected from at the 9th level of the San Antonio mine in 2017 and was obtained by one of the authors (MS) from mineral collector Gerardo Pérez Reveles and later donated to the collections of National Museum in Prague.

Fig. 1 *Outline map of Mexico with States of Federation as well as approximate positions of localities MSA and FIM indicated.*

Table 1 *Lattice parameters (in Å, with standard uncertainties in parentheses), OD subfamilies (Bailey's groups), and polytypes of selected crystals of cronstedtite from San Antonio mine (MSA), Mexico*

Sample	*a*	*b*	*c*	Volume	Group	Polytype(s)	Note
CD_1	5.5015(8)	5.5015(8)	21.287(3)	557.96(14)	A	3*T*	Obv.-rev. twin, 2-nd domain weak
CD_2	5.5037(7)	5.5037(7)	21.308(3)	558.95(12)	A	3*T*	Obv.-rev. twin, 2-nd domain weaker., Fig. 3
CD_3	5.5076(7)	5.5076(7)	14.2079(19)	373.23(8)	D	$2H_1$+$2H_2$+$6T_1$?	$2H_2$ weak, possible content of $6T_1$, EPMA
CD_4	5.5003(8)	5.5003(8)	21.282(3)	557.58(13)	A	3*T*	
CD_5	5.4964(9)	5.4964(9)	14.189(2)	371.23(11)	D	$2H_1$(+$2H_2$)	$2H_2$ very weak
CD_6	5.4991(7)	5.4991(7)	21.261(3)	556.79(13)	A	3*T*	Obverse-reverse twin, EPMA
CD_7	5.4926(9)	5.4926(9)	14.192(2	370.78(11)	D	$2H_1$(+$2H_2$)	$2H_2$ very weak
CD_8	5.5007(7)	5.5007(7)	21.283(3)	557.68(13)	A	3*T*	
CD_9	5.5072(8)	5.5072(8)	21.299(3)	559.42(14)	A	3*T*	
CD_10	5.5046(7)	5.5046(7)	21.286(3)	558.58(13)	A	3*T*	
CD_11	5.5071(7)	5.5071(7)	21.307(3)	559.62(13)	A	3*T*	
CD_12	5.5031(7)	5.5031(7)	21.295(3)	558.50(13)	A	3*T*	
CD_13	5.5020(7)	5.5020(7)	21.288(3)	558.08(13)	A	3*T*	Obv.-rev. twin, 2-nd domain weak, EPMA
CD_14	5.5026(9)	5.5026(9)	21.291(4)	558.29(16)	A	3*T*	Diff. streaks, misorented domains
CD_15	5.4932(9)	5.4932(9)	21.360(4)	558.19(17)	A + D	3*T* +$2H_1$	A+D accretion, part 3*T*, obv.-rev. twin
	5.4969(14)	5.4969(14)	14.206(4)	371.74(17)			A+D accretion, part $2H_1$,
CD_16	5.5020(8)	5.5020(8)	21.290(3)	558.13(14)	A	3*T*	Slight diffuse streaks
CD_17	5.5037(6)	5.5037(6)	21.274(2)	558.07(10)	A	3*T*	Slight diffuse streaks
BD_1	5.5010(8)	5.5010(8)	21.297(3)	558.11(14)	A	3*T*	Slight diffuse streaks
BD_2	5.5062(8)	5.5062(8)	21.296(4)	559.16(16)	A	3*T*	Obv.-rev. twin, 2-nd domain weak
BD_3	5.5103(8)	5.5103(8)	21.319(3)	560.58(14)	A	3*T*	Obv.-rev. twin, dtto
BD_4	5.5089(6)	5.5089(6)	21.312(3)	560.11(12)	A	3*T*	Obv.-rev. twin, dtto
BD_5	5.5045(8)	5.5045(8)	21.306(3)	559.07(13)	A	3*T*	Slight diffuse streaks
BD_6	5.5037(9)	5.5037(9)	21.278(4)	558.20(17)	A	3*T*	Obverse-reverse twin, EPMA
BD_7	5.5083(7)	5.5083(7)	21.310(3)	559.95(13)	A	3*T*	
BD_8	5.5088(8)	5.5088(8)	21.319(4)	560.27(16)	A	3*T*	Slight diffuse streaks
BD_9	5.5013(7)	5.5013(7)	21.301(3)	558.28(13)	A	3*T*	Slight diffuse streaks, EPMA
BD_10	5.5060(7)	5.5060(7)	21.301(3)	559.27(13)	A	3*T*	Slight diffuse streaks
BD_11	5.5057(10)	5.5057(10)	21.304(4)	559.25(18)	A	3*T*	Slight diffuse streaks
BD_12	5.5037(8)	5.5037(8)	21.305(3)	558.87(14)	A	3*T*	Slight diffuse streaks
BD_13	5.5058(8)	5.5058(8)	21.299(3)	559.17(13)	A	3*T*	Slight diffuse streaks
PY_3	5.5069(7)	5.5069(7)	21.324(3)	560.04(13)	A	3*T*	Diffuse streaks
PY_6	5.5015(7)	5.5015(7)	21.285(3)	557.93(13)	A	3*T*	Diffuse streaks
PY_7	5.5107(7)	5.5107(7)	21.321(3)	560.74(13)	A	3*T*	Diff. streaks, misoriented domains
PY_8	5.5071(7)	5.5071(7)	21.309(3)	559.67(12)	A	3*T*	Diffuse streaks

The Francisco I. Madero mine is located approximately 17 km WNW of the Zacatecas city, Zacatecas Municipality, Zacatecas State, Mexico (Fig. 1). GPS coordinates of the mine are: 22°49'20.6"N 102°43'53.3"W. The Francisco I. Madero Zn-Cu-Pb-Ag deposit is hosted in Cretaceous limestone-shale sequence and it is consisting of sphalerite rich mantos at the base and garnet-hedenbergite, epidote or pyroxene ore skarns with sphalerite, galena, pyrite and chalcopyrite at the top of the orebody (Canet et al. 2009a, b). Other authors (e.g. Camprubí et al. 2017) consider this deposit to be of the SEDEX origin. Superb groups and clusters of cronstedtite crystals up to 1.5 cm long were collected at zone 43 of the mine in late 2018. A small cluster of cronstedtite crystals (FIM in the following) from this find was obtained by author (MS) from mineral collector Gerardo Pérez Reveles and was later donated for this research.

Experimental

Single crystal X-ray diffraction

Crystal fragments were selected under the stereomicroscope and mounted onto the glass fibre. Then they were studied by the single crystal X-ray diffraction with aid of the four-circle (double-wavelength) X-ray diffractometer Gemini A Ultra (Rigaku Oxford Diffraction) equipped with the CCD area detector Atlas S2 in the Institute of Physics, Czech Academy of Sciences. The Mo*K*α radiation with λ = 0.71070 Å with graphite monochromator and enhance fiber optics collimator was used.

The pre-experiment was performed first, followed by the full experiment covering the whole sphere. Such experiment required typically tens of minutes or few hours. The CrysAlisPro version 171.41.93a (Rigaku Oxford Diffraction 2021) package was used for the data collection,

Table 2 *Lattice parameters (in Å, with standard uncertainties in parentheses), OD subfamilies (Bailey's groups), and polytypes of selected crystals of cronstedtite from Francisco I. Madero Mine (FIM), Mexico*

Sample	*a*	*b*	*c*	Volume	Group	Polytype(s)	Note
FIM_1	5.4638(19)	5.4638(19)	14.177(6)	366.5(2)	D	$2H_2$	Misorient. domains, EPMA
FIM_2	5.4613(19)	5.4613(19)	14.035(4)	362.5(2)	D	$2H_2$?	Misoriented domains
FIM_3	5.4782(14)	5.4782(14)	14.126(4)	367.15(16)	D	$2H_2$+$2H_1$	Diffuse streaks
FIM_4	5.4640(16)	5.4640(16)	14.112(4)	364.86(18)	D	$2H_2$?	Misoriented domains
FIM_5	5.483(3)	5.483(3)	21.211(15)	552.2(6)	A	$3T$	Misoriented domains
FIM_6	5.479(2)	5.479(2)	14.159(6)	368.0(3)	D	$2H_2$+$2H_1$	Misoriented domains
FIM_7	5.4792(15)	5.4792(15)	14.133(4)	367.46(18)	D	$2H_2$+$2H_1$	Diffuse streaks, EPMA
FIM_8	5.4798(15)	5.4798(15)	14.127(4)	367.37(18)	D	$2H_2$+$2H_1$	Misoriented domains
FIM_9	5.4779(12)	5.4779(12)	14.129(4)	367.16(15)	D	$2H_2$+$2H_1$	Diff. streaks arc shap. refl.
FIM_10	5.4765(13)	5.4765(13)	14.131(4)	367.03(16)	D	$2H_2$+$2H_1$	Diffuse streaks
FIM_11	5.4785(17)	5.4785(17)	14.124(6)	367.1(2)	D	disordered	Diffuse, subfam. structure
FIM_12	5.4799(15)	5.4799(15)	14.132(4)	367.52(17)	D	$2H_2$+$2H_1$	Diff. streaks arc shap. refl.
FIM_13	5.474(2)	5.474(2)	21.200(10)	550.2(4)	A	$3T$	Diff. streaks arc shap. refl.
FIM_14	5.4808(15)	5.4808(15)	14.166(4)	368.51(18)	D	$2H_2$+$2H_1$	
FIM_15	5.466(2)	5.466(2)	14.185(7)	367.1(3)	D	$2H_2$+$2H_1$	Diff. streaks misor. domains
FIM_16	5.466(3)	5.466(3)	14.132(9)	365.7(4)	D	$2H_2$+$2H_1$	Diff. streaks arc shap. refl.
FIM_17	5.427(7)	5.427(7)	14.193(15)	362.1(7)	D	$2H_2$+$2H_1$	Arc shaped reflexions
FIM_18	5.4837(16)	5.4837(16)	14.139(5)	368.2(2)	D	$2H_2$+$2H_1$	Arc shaped reflections
FIM_19	5.5142(13)	5.5142(13)	14.174(4)	373.24(16)	D	$2H_2$+$2H_1$	Diffuse streaks
FIM_20	5.5026(6)	5.5026(6)	14.1983(16)	372.31(7)	D	$2H_2$+$2H_1$(+$6T_1$?)	Diffuse streaks, $6T_1$ weak
FIM_21	5.4999(5)	5.4999(5)	14.1881(16)	371.68(7)	D	$2H_2$+$2H_1$	Diffuse streaks, EPMA
FIM_22	5.5046(6)	5.5046(6)	14.1993(16)	372.60(7)	D	$2H_2$+$2H_1$	pseudo-twin about c by ~ 18°
FIM_23	5.5117(9)	5.5117(9)	14.220(2)	374.11(11)	D	$2H_2$+$2H_1$	Misoriented domains
FIM_24	5.5028(7)	5.5028(7)	14.1875(18)	372.05(8)	D	$2H_2$+$2H_1$(+?)	Accessory of $6T_1$, $6R_2$?
FIM_25	5.5041(4)	5.5041(4)	14.1974(11)	372.49(5)	D	$2H_2$+$2H_1$	Diffuse streaks
FIM_26	5.5056(4)	5.5056(4)	14.2044(12)	372.87(5)	D	$2H_2$+$2H_1$	Diffuse streaks
FIM_27	5.5192(7)	5.5192(7)	14.231(2)	375.42(8)	D	$2H_2$+$2H_1$	Diffuse streaks, Fig. 4
FIM_28	5.4960(9)	5.4960(9)	21.213(3)	554.92(16)	A	$3T$	Diffuse streaks, EPMA
FIM_29	5.4995(10)	5.4995(10)	14.169(2)	371.12(11)	D	$2H_2$+$2H_1$ (+$6T_1$?)	Base part of trunc. cone
FIM_29_1	5.5023(6)	5.5023(6)	42.568(5)	1116.1(2)	D	$6T_1$	Cleaved part of FIM_29, Fig. 5
FIM_29_2	5.5049(5)	5.5049(5)	42.600(3)	1118.00(18)	D	$6T_1$	Cleaved part of FIM_29
FIM_29_3	5.5051(7)	5.5051(7)	42.554(6)	1116.8(2)	D	($6T_1$)	Cleaved part of FIM_29
FIM_29_4	5.5028(5)	5.5028(5)	42.568(4)	1116.30(18)	D	($6T_1$)	Cleaved part of FIM_29
FIM_30	5.5038(11)	5.5038(11)	21.305(5)	558.9(2)	A	3T (+$6T_2$?)	$6T_2$ questionable
FIM_31	5.5051(11)	5.5051(11)	42.571(8)	1117.3(4)	D	$6T_1$, (+$2H_2$?)	Base part of trunc. cone

unit cell parameters calculation, and processing of data recorded. Thirty four fragments from MSA and 31 from FIM were tested altogether. One crystal from FIM was cleaved into smaller parts and these fragments were later studied separately. The "unwarp" procedure was used for processing of datasets and generating of user-defined images of reciprocal space sections (RS sections in the following), equivalents of precession photographs.

The RS sections corresponding to six important reciprocal lattice planes were created: $(2\bar{h}\bar{h}l_{hex})^*$, $(hhl_{hex})^*$, $(\bar{h}2hl_{hex})^*$, $(h0l_{hex})^*$, $(0kl_{hex})^*$, and $(\bar{h}hl_{hex})^*$. Distributions of so-called subfamily reflections along the reciprocal lattice rows $[2\bar{1}l]^*$ / $[11l]^*$ / $[\bar{1}2l]^*$ in $(2\bar{h}\bar{h}l_{hex})^*$ / $(hhl_{hex})^*$ / $(\bar{h}2hl_{hex})^*$ planes, respectively, are used to determine OD subfamilies (Bailey's groups) A, B, C, D (Dornberger-Schiff, Ďurovič 1975a, b; Bailey 1969; 1988). Similarly, distributions of characteristic reflections along $[10l]^*$ / $[01l]^*$ / $[\bar{1}1l]^*$rows in $(h0l_{hex})^*$ / $(0kl_{hex})^*$ / $(\bar{h}hl_{hex})$ RS sections were used to determine polytypes. Graphical identification diagrams published e.g. by Mikloš (1975), Ďurovič (1981, 1997), Weiss, Kužvart (2005), and extended by Hybler et al. (2018, 2021b) were used for a simple visual comparison with real diffraction patterns. Unit-cell parameters of selected samples are summarized in Tables 1 and 2.

Electron probe microanalysis

The selected fragments of cronstedtite crystals, in which polytypes were determined, were mounted to epoxy discs, polished by diamond suspensions and coated with carbon layer of about 30 nm in thick. The polished grains were analysed at the National Museum in Prague using a CAMECA SX-100 electron probe microanalyzer operating in wave-dispersive (WDS) mode with acceleration voltage of 15 kV, beam current of 10 nA and beam diameter of 5 μm. The following standards and analytical lines were used: hematite (Fe*K*α), albite (Na*K*α), baryte (Ba*L*α), fluorapatite (P*K*α), ce-

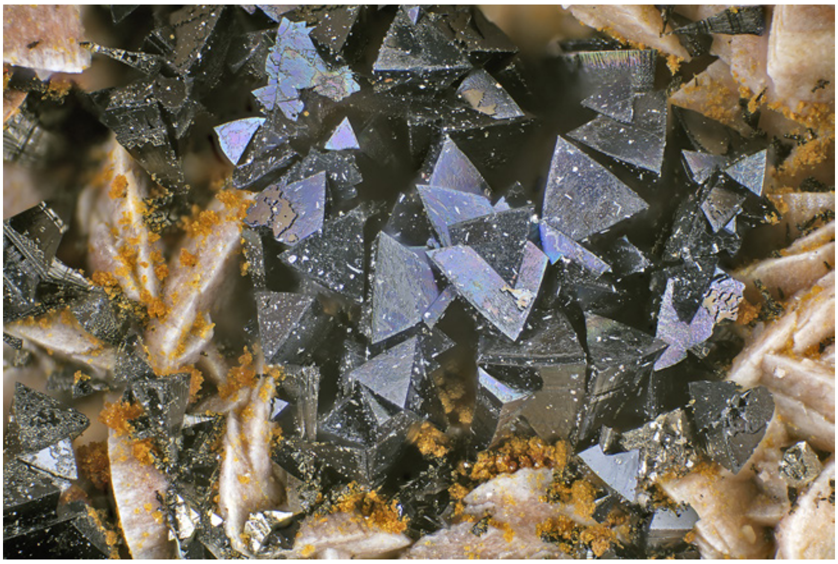

Fig. 2 *Group of black crystals of cronstedtite-3T resting with minor pyrite on siderite, San Antonio mine (MSA), Mexico (National Museum, Prague, catalogue No P1N114456). Photo Pavel Škácha, field of view 4 mm.*

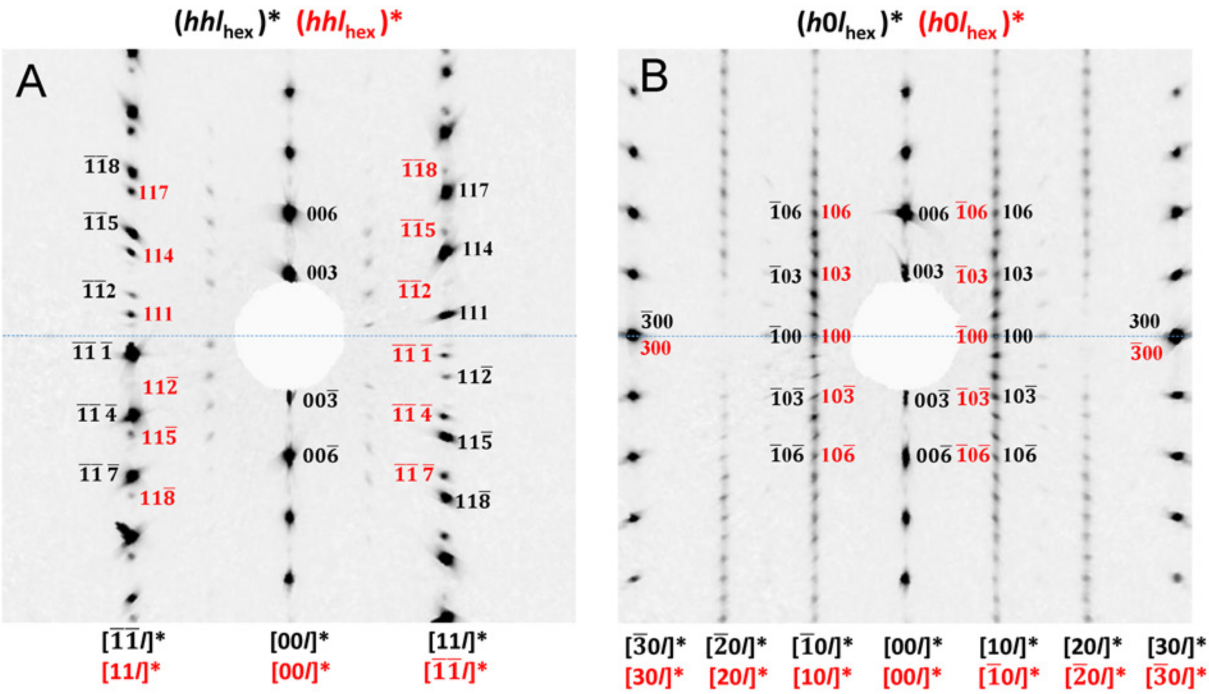

Fig. 3 *RS sections of the* 3*T polytype - subfamily* A, *from San Antonio mine (MSA), Mexico.* a) *The* $(hhl_{hex})^*$ *section, subfamily* A, *"obverse-reverse twin". Indices of reflections and symbols of reciprocal lattice rows and planes of the first and second twin individuals are in black and red colours, respectively. Indices of reflections in the* [00*l*]* *row are identical for both twin individuals.* b) *The* $(h0l_{hex})^*$ *RS section of the polytype* 3*T.*

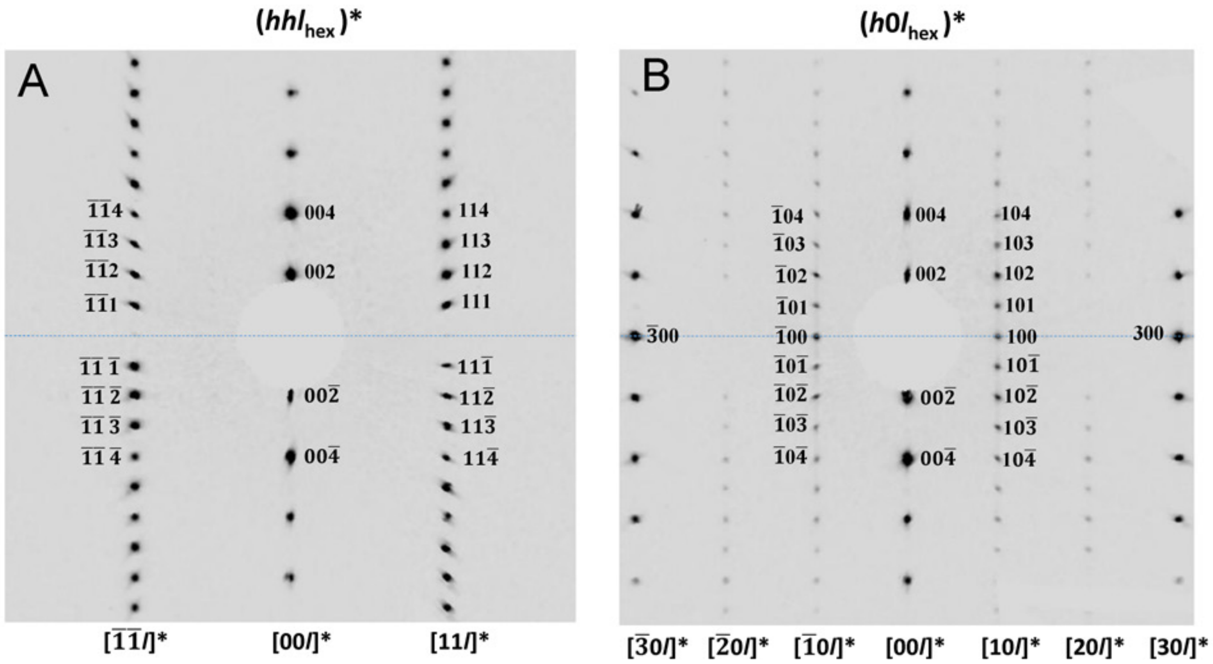

Fig. 4 *RS sections of the* $2H_2$ *polytype - subfamily* D*, possible allotwin with* $2H_1$*, FIM locality.* a) *The* $(hhl_{hex})^*$ *section, indices of selected reflections and symbols of reciprocal lattice rows and planes are indicated.* b) *The* $(h0l_{hex})^*$ *RS section of the same crystal. Selected characteristic reflections in the* $[\bar{1}0l]^*$ *and* $[10l]^*$ *rows and some other ones are indicated. Note that both RS sections are indexed with respect of two-layer polytype(s).*

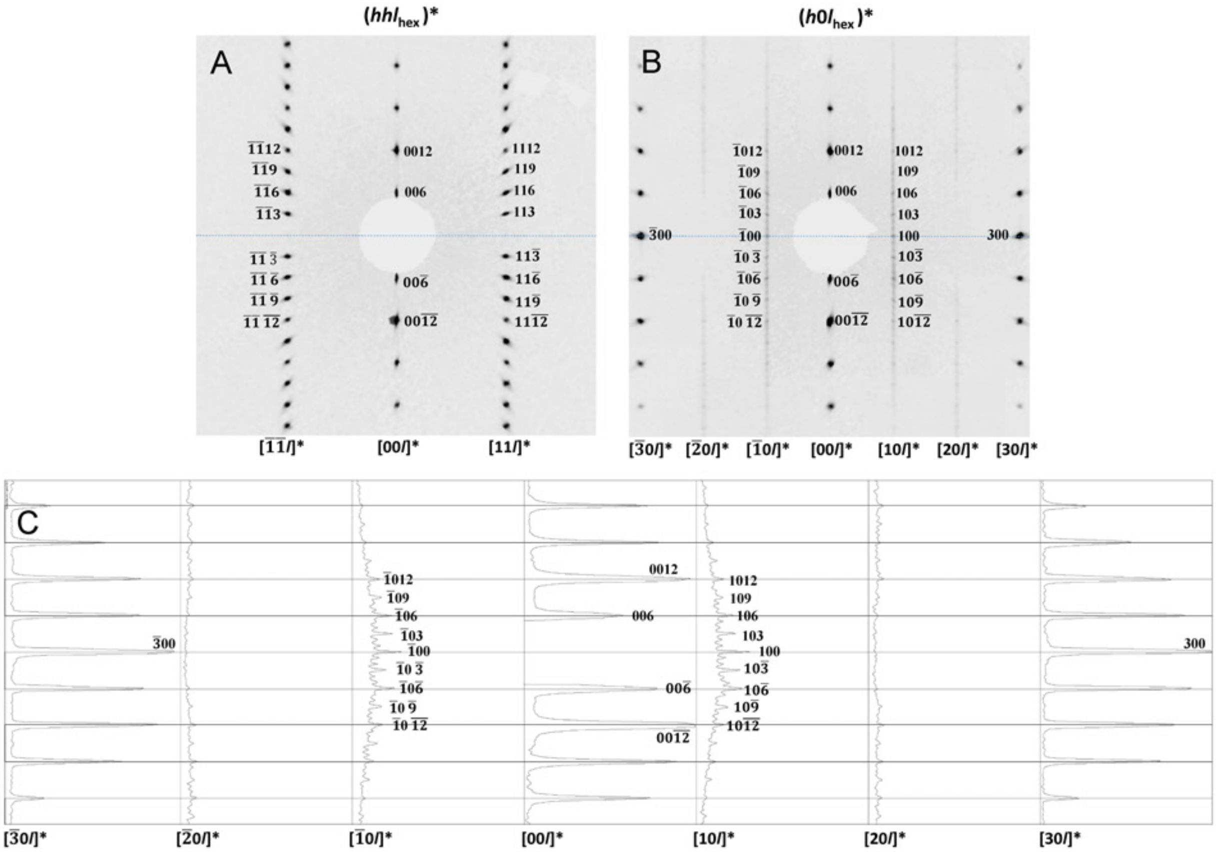

Fig. 5 *The* $6T_1$ *polytype - subfamily* D*, FIM locality. Note that both RS sections are now indexed with respect of the six-layer polytype.* a) *The* $(hhl_{hex})^*$ *section, indices of selected reflections and symbols of reciprocal lattice rows and planes are indicated.* b) *The* $(h0l_{hex})^*$ *RS section of the same crystal. Note the distribution of reflections in the* $[\bar{1}0l]^*$ *and* $[10l]^*$ *rows, corresponding to the six-layer periodicity. The* $l = 3n$ *are significantly stronger, than other in rows* $[\bar{1}0l]^*$ *and* $[10l]^*$. c) *Curves of integrated intensities along rows the* $(h0l_{hex})^*$ *RS section (previous image). Indices of selected peaks corresponding to respective reflections are indicated. Note stronger* $l = 3n$ *and weaker* $l = 3n+1$ *and* $l = 3n+2$ *peaks in the* $[\bar{1}0l]^*$ *and* $[10l]^*$ *curves. In second-order rows* $[\bar{2}0l]^*$ and $[20l]^*$ *the* $l = 3n$ *reflections and respective peaks in curves are recognizable, while the weak reflections are hidden in the noise due to the partial stacking disorder. The* $[\bar{3}0l]^*$, $[00l]^*$, $[30l]^*$ *rows contain the strong and sharp subfamily reflections.*

lestite (S*K*α), Co (Co*K*α), Cr_2O_3 (Cr*K*α), diopside (Mg*K*α), halite (Cl*K*α), chalcopyrite (Cu*K*α), LiF (F*K*α), rhodonite (Mn*K*α), sanidine (K*K*α, Al*K*α), TiO_2 (Ti*K*α), vanadinite (V*K*α), wollastonite (Si*K*α, Ca*K*α) and ZnO (Zn*K*α). The peak counting times were between 10 and 20 s and half of the peak time was used for both background positions. The raw counts were converted to wt. % using the standard PAP procedure (Pouchou and Pichoir 1985). Oxygen was calculated from stoichiometry. The above listed elements, which are not included in the tables, were in all cases below the limits of detection. The contents of H_2O, Fe^{2+} and Fe^{3+} as well as *x*-values were calculated on the basis of general formula of cronstedtite $(Fe^{2+}_{3-x}Fe^{3+}_{x})(Si_{2-x}Fe^{3+}_{x})O_5(OH)_4$.

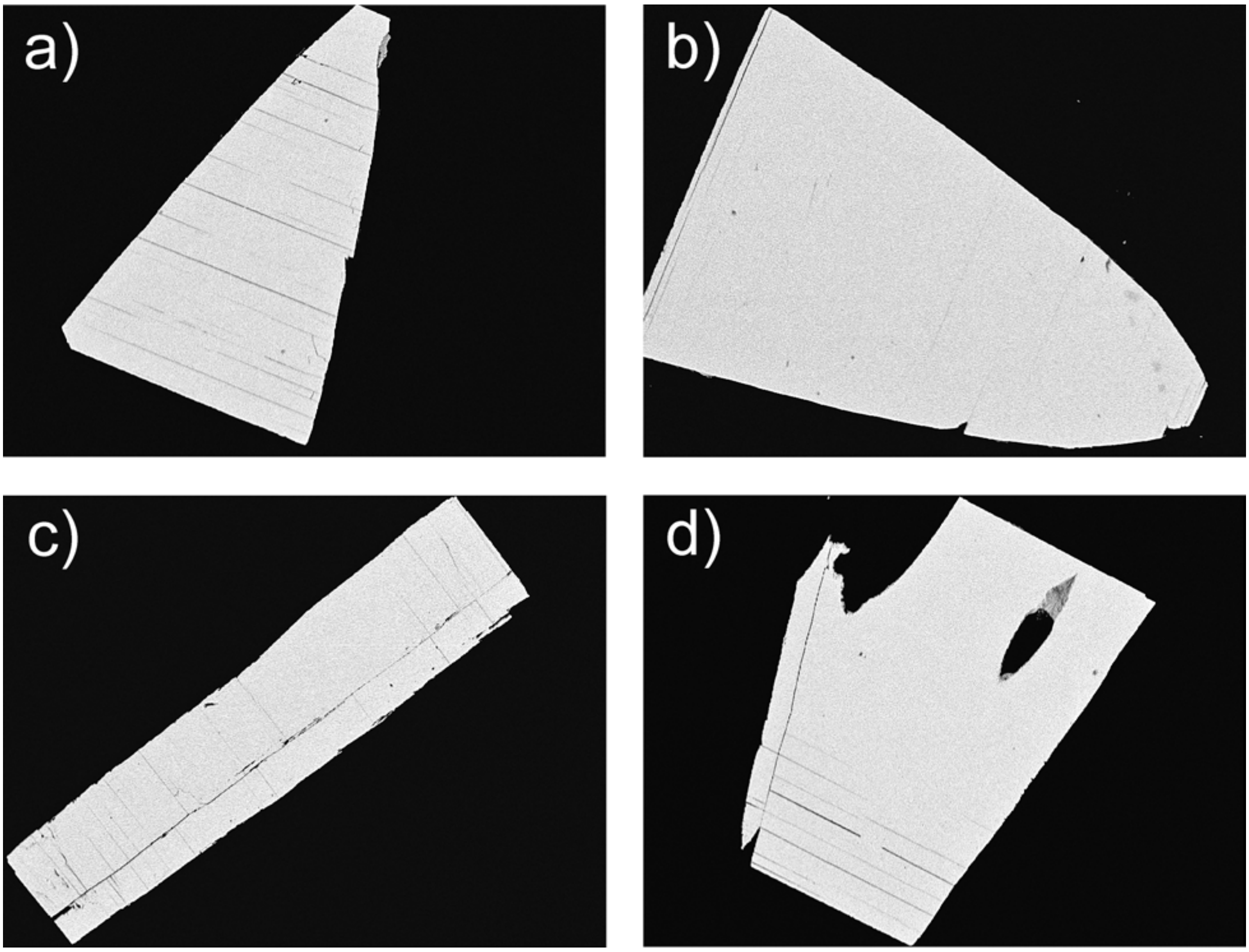

Fig. 6 *Appearance of studied polished cronstedtite crystals on BSE images - samples a) MSABD9 polytype 3T, FOV (field of view) 800 µm; b) MSACD3 polytype* $2H_1+2H_2+6T_1$*?, FOV 800 µm; c) F1M1 polytype* $2H_2$*, FOV 1700 µm; d) F1M28 polytype 3T, FOV 900 µm; BSE photos Z. Dolníček.*

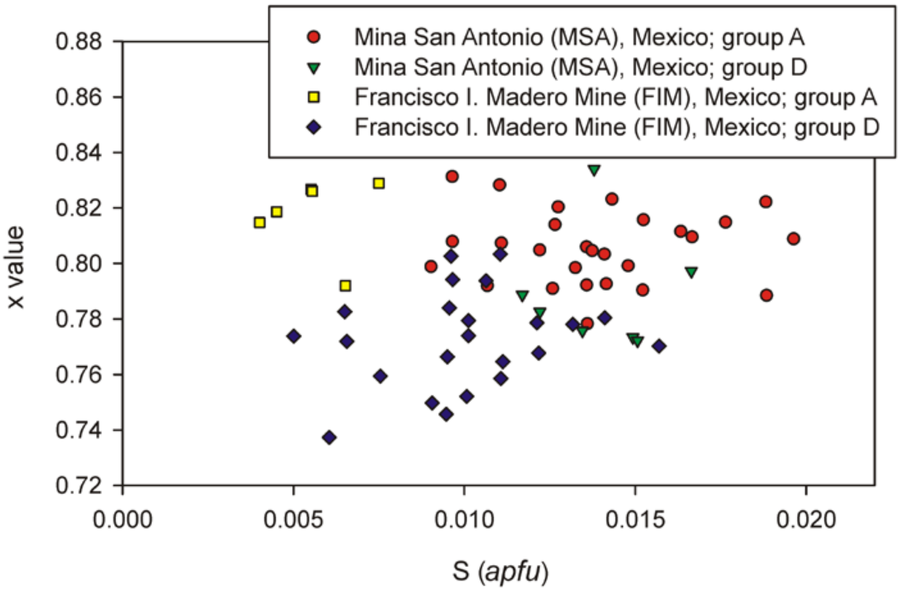

Fig. 7 *Sulphur (apfu) vs. x value (of ideal formula) for studied cronstedtite; group - OD subfamilies (Bailey's groups).*

Results and discussion

Polytypes found

San Antonio mine (MSA)

The sample *San Antonio mine* (MSA, National Museum catalogue No. P1N114456) is composed of pyrite mass on the silicate substrate covered by spherical or irregular aggregates of siderite. Cronstedtite forms druses filling space between these aggregates (Fig. 2). Some cronstedtite crystals are embedded in pyrite.

Three batches of specimens were selected: i) from the central druse (CD in the following), ii) from another druse at the back side of the sample (BD), iii) from pyrite (PY). All crystals selected were euhedral, or fragments of larger euhedral crystals.

The polytype 3*T* of the subfamily - Bailey´s group A is dominant in all three batches of crystals studied (Fig. 3). In the BD and PY batches the 3*T* polytype was the only polytype found. Several crystals were twinned by reticular merohedry with the 180° rotation as twinning operation. This operation exchanges obverse and reverse settings of the subset of so-called subfamily reflections. This phenomenon is visible in $(2h\bar{h}l_{hex})^*$ / $(hhl_{hex})^*$ / $(\bar{h}2hl_{hex})^*$ planes. The example is presented in Figure 3a. This kind of twinning affects all polytypes of the A subfamily and is widespread (Hybler et al. 2016, 2017, 2020, 2021b; Hybler and Sejkora 2017).

Table 3 *Chemical composition of selected fragments of cronstedtite from the San Antonio mine (* calculated from stoichiometry)*

			wt.%						*apfu*					
sample			FeO	Fe_2O_3	SiO_2	S	H_2O*	total	Fe^{2+}	Fe^{3+}	Si	S	OH	x
MSABD6	A	3*T*	38.74	31.57	17.64	0.10	8.80	96.85	2.195	1.610	1.195	0.012	3.976	0.80
MSABD6	A	3*T*	38.38	32.11	17.37	0.10	8.77	96.73	2.180	1.641	1.180	0.013	3.975	0.82
MSABD6	A	3*T*	39.20	31.29	17.93	0.11	8.84	97.37	2.207	1.585	1.207	0.014	3.972	0.79
MSABD6	A	3*T*	39.10	31.09	17.90	0.12	8.81	97.01	2.210	1.581	1.210	0.015	3.970	0.79
MSABD6	A	3*T*	38.99	31.09	17.84	0.08	8.81	96.81	2.208	1.584	1.208	0.011	3.979	0.79
MSABD6	A	3*T*	38.72	31.25	17.67	0.12	8.76	96.52	2.201	1.598	1.201	0.015	3.970	0.80
mean			38.86	31.40	17.73	0.10	8.80	96.88	2.200	1.600	1.200	0.013	3.973	0.80
MSABD9	A	3*T*	38.49	31.73	17.48	0.13	8.75	96.57	2.188	1.623	1.188	0.016	3.967	0.81
MSABD9	A	3*T*	39.18	31.99	17.83	0.11	8.89	98.00	2.194	1.612	1.194	0.014	3.973	0.81
MSABD9	A	3*T*	38.77	32.09	17.59	0.10	8.84	97.38	2.186	1.628	1.186	0.013	3.975	0.81
MSABD9	A	3*T*	39.60	30.83	18.21	0.11	8.88	97.63	2.222	1.557	1.222	0.014	3.973	0.78
MSABD9	A	3*T*	38.87	32.96	17.54	0.09	8.93	98.39	2.172	1.657	1.172	0.011	3.978	0.83
MSABD9	A	3*T*	38.72	31.54	17.63	0.11	8.78	96.78	2.195	1.609	1.195	0.014	3.973	0.80
MSABD9	A	3*T*	38.74	31.74	17.62	0.08	8.82	97.00	2.192	1.616	1.192	0.010	3.981	0.81
mean			38.91	31.84	17.70	0.10	8.84	97.39	2.193	1.615	1.193	0.013	3.974	0.81
MSACD3	D	$2H_1+2H_2+6T_1$?	39.03	30.94	17.88	0.09	8.80	96.75	2.211	1.577	1.211	0.012	3.977	0.79
MSACD3	D	$2H_1+2H_2+6T_1$?	40.06	31.06	18.44	0.11	8.97	98.64	2.224	1.552	1.224	0.013	3.973	0.78
MSACD3	D	$2H_1+2H_2+6T_1$?	40.16	31.00	18.50	0.12	8.98	98.76	2.227	1.547	1.227	0.015	3.970	0.77
MSACD3	D	$2H_1+2H_2+6T_1$?	39.12	30.69	17.96	0.10	8.79	96.65	2.217	1.565	1.217	0.012	3.976	0.78
MSACD3	D	$2H_1+2H_2+6T_1$?	39.81	30.67	18.35	0.12	8.89	97.85	2.228	1.544	1.228	0.015	3.970	0.77
MSACD3	D	$2H_1+2H_2+6T_1$?	39.20	31.54	17.90	0.13	8.85	97.62	2.203	1.595	1.203	0.017	3.967	0.80
MSACD3	D	$2H_1+2H_2+6T_1$?	38.05	32.57	17.13	0.11	8.75	96.61	2.166	1.668	1.166	0.014	3.972	0.83
mean			39.35	31.21	18.02	0.11	8.86	97.55	2.211	1.578	1.211	0.014	3.972	0.79
MSACD6	A	3*T*	39.40	31.78	17.98	0.07	8.94	98.17	2.201	1.598	1.201	0.009	3.982	0.80
MSACD6	A	3*T*	38.91	32.25	17.65	0.14	8.85	97.81	2.185	1.630	1.185	0.018	3.965	0.81
MSACD6	A	3*T*	39.07	31.97	17.77	0.09	8.89	97.78	2.193	1.615	1.193	0.011	3.978	0.81
MSACD6	A	3*T*	38.34	32.67	17.28	0.08	8.82	97.19	2.169	1.663	1.169	0.010	3.981	0.83
MSACD6	A	3*T*	38.94	31.99	17.70	0.13	8.84	97.61	2.190	1.619	1.190	0.017	3.967	0.81
MSACD6	A	3*T*	39.07	32.05	17.76	0.16	8.85	97.89	2.191	1.618	1.191	0.020	3.961	0.81
MSACD6	A	3*T*	39.39	31.35	18.03	0.10	8.89	97.76	2.209	1.582	1.209	0.013	3.975	0.79
mean			39.02	32.01	17.74	0.11	8.87	97.74	2.191	1.618	1.191	0.014	3.972	0.81
MSACD13	A	3*T*	38.98	30.90	17.86	0.15	8.76	96.64	2.211	1.577	1.211	0.019	3.962	0.79
MSACD13	A	3*T*	38.78	31.26	17.70	0.10	8.78	96.62	2.202	1.597	1.202	0.013	3.974	0.80
MSACD13	A	3*T*	38.60	32.04	17.50	0.12	8.79	97.05	2.184	1.631	1.184	0.015	3.970	0.82
MSACD13	A	3*T*	38.43	32.24	17.38	0.15	8.77	96.97	2.178	1.644	1.178	0.019	3.962	0.82
MSACD13	A	3*T*	39.16	31.83	17.84	0.11	8.88	97.82	2.197	1.607	1.197	0.014	3.972	0.80
MSACD13	A	3*T*	39.41	31.43	18.03	0.11	8.89	97.87	2.208	1.584	1.208	0.014	3.973	0.79
MSACD13	A	3*T*	38.20	32.11	17.27	0.11	8.74	96.43	2.177	1.646	1.177	0.014	3.971	0.82
mean			38.79	31.69	17.65	0.12	8.80	97.06	2.194	1.612	1.194	0.015	3.969	0.81

Most of characteristic reciprocal space rows are slightly diffusely streaked.

In the CD batch, three specimens were $2H_1$ polytypes with small amount of $2H_2$ of the subfamily D. In the CD_3 sample, a small amount of $6T_1$ polytype is possible. The CD_15 sample contains both $3T$ + $2H_1$ polytypes of A and D subfamilies, respectively. However, the microscopic check revealed that the specimen was not a true allotwin, but rather an accretion of two distinct crystal individuals.

Francisco I. Madero mine (FIM)

From this locality, a batch of selected fragments was available. Specimens for studies were selected under the stereomicroscope. In some cases, crystals were further fragmented in order to obtain specimens of appropriate size. All specimens selected were euhedral crystals or fragments of larger euhedral crystals.

Most crystals belong to the subfamily D, represented mostly by $2H_2$+$2H_1$ polytypes in various allotwins (Fig. 4). The $3T$ polytype (subfamily A) was recorded, too, but occurs rarely. The lowermost part of the pyramid of one crystal (FIM_29) was somewhat differently coloured (more brownish) than the rest of the crystal. It has been cleaved out and fell into pieces. Their X-ray studies revealed the six-layer polytype $6T_1$ (Fig. 5). The [$10l$]* and [$\bar{1}0l$]* rows in the ($h0l_{hex}$)* image are six times densely occupied by weak reflections while every third reflection (l = 3n) is somewhat stronger than others. This arrangement corresponds to the first one of 24 possible sequences of six-layer polytypes as derived by Hall et al. (1976). Later Hybler et al. (2021a) derived theoretical diffraction patterns of all 24 Hall's sequences and identified some other six-layer polytypes. Curves of integrated intensities along rows the ($h0l_{hex}$)* RS section were recorded (Fig. 5c). The characteristic property of the diffraction pattern (every third reflection along [$10l$]* and [$\bar{1}0l$]* rows stronger) is evident. This arrangement of reflection is obeyed also for [$\bar{2}0l$]* and [$20l$]* rows, however, all but the strongest (l = 3n) are hidden in the noise.

Table 4 *Chemical composition of selected fragments of cronstedtite from the Francisco I. Madero Mine (* calculated from stoichiometry)*

			wt.%								*apfu*						
sample			FeO	Fe_2O_3	SiO_2	S	Cl	H_2O*	O=Cl	total	Fe^{2+}	Fe^{3+}	Si	S	Cl	OH	x
FIM7	D	$2H_2$+$2H_1$	39.79	31.22	18.27	0.05	0.04	8.96	-0.01	98.32	2.217	1.565	1.217	0.007	0.005	3.982	0.78
FIM7	D	$2H_2$+$2H_1$	40.57	29.83	18.88	0.08	0.05	8.97	-0.01	98.37	2.254	1.491	1.254	0.009	0.006	3.975	0.75
FIM7	D	$2H_2$+$2H_1$	40.00	30.13	18.52	0.06	0.00	8.92	0.00	97.63	2.241	1.519	1.241	0.008	0.000	3.985	0.76
FIM7	D	$2H_2$+$2H_1$	40.05	30.55	18.50	0.08	0.05	8.94	-0.01	98.15	2.234	1.533	1.234	0.010	0.006	3.975	0.77
FIM7	D	$2H_2$+$2H_1$	39.98	30.07	18.52	0.09	0.04	8.89	-0.01	97.58	2.241	1.517	1.241	0.011	0.005	3.973	0.76
FIM7	D	$2H_2$+$2H_1$	39.52	30.35	18.23	0.12	0.06	8.80	-0.01	97.07	2.230	1.540	1.230	0.016	0.007	3.962	0.77
FIM7	D	$2H_2$+$2H_1$	39.90	30.83	18.38	0.04	0.05	8.95	-0.01	98.14	2.226	1.548	1.226	0.005	0.006	3.984	0.77
FIM7	D	$2H_2$+$2H_1$	39.51	31.06	18.13	0.08	0.04	8.89	-0.01	97.70	2.216	1.568	1.216	0.010	0.005	3.976	0.78
FIM7	D	$2H_2$+$2H_1$	38.97	31.64	17.76	0.08	0.00	8.85	0.00	97.30	2.197	1.605	1.197	0.010	0.000	3.981	0.80
mean			39.81	30.63	18.35	0.07	0.04	8.91	-0.01	97.81	2.229	1.543	1.229	0.009	0.004	3.977	0.77
FIM1	D	$2H_2$	39.38	30.72	18.10	0.08	0.04	8.84	-0.01	97.14	2.221	1.559	1.221	0.010	0.005	3.975	0.78
FIM1	D	$2H_2$	40.28	29.18	18.80	0.05	0.04	8.89	-0.01	97.24	2.263	1.475	1.263	0.006	0.005	3.983	0.74
FIM1	D	$2H_2$	39.54	30.90	18.17	0.11	0.06	8.86	-0.01	97.63	2.220	1.561	1.220	0.014	0.007	3.965	0.78
FIM1	D	$2H_2$	39.25	31.90	17.88	0.09	0.05	8.90	-0.01	98.05	2.197	1.607	1.197	0.011	0.006	3.972	0.80
FIM1	D	$2H_2$	39.61	30.51	18.26	0.05	0.06	8.87	-0.01	97.35	2.228	1.544	1.228	0.007	0.007	3.980	0.77
FIM1	D	$2H_2$	39.36	30.63	18.10	0.10	0.04	8.81	-0.01	97.04	2.222	1.556	1.222	0.013	0.005	3.969	0.78
FIM1	D	$2H_2$	39.49	30.19	18.23	0.10	0.05	8.80	-0.01	96.84	2.232	1.535	1.232	0.012	0.006	3.970	0.77
mean			39.56	30.58	18.22	0.08	0.05	8.85	-0.01	97.33	2.226	1.548	1.226	0.010	0.006	3.974	0.77
FIM21	D	$2H_2$+$2H_1$	38.94	31.16	17.80	0.08	0.07	8.79	-0.02	96.82	2.206	1.588	1.206	0.010	0.008	3.973	0.79
FIM21	D	$2H_2$+$2H_1$	39.47	30.75	18.15	0.10	0.06	8.84	-0.01	97.36	2.221	1.557	1.221	0.012	0.007	3.969	0.78
FIM21	D	$2H_2$+$2H_1$	39.47	30.50	18.18	0.08	0.07	8.83	-0.02	97.12	2.226	1.548	1.226	0.010	0.008	3.972	0.77
FIM21	D	$2H_2$+$2H_1$	39.10	31.27	17.88	0.08	0.05	8.83	-0.01	97.21	2.206	1.588	1.206	0.011	0.006	3.973	0.79
FIM21	D	$2H_2$+$2H_1$	39.66	30.15	18.33	0.09	0.05	8.84	-0.01	97.11	2.235	1.529	1.235	0.011	0.006	3.972	0.76
FIM21	D	$2H_2$+$2H_1$	40.06	29.80	18.60	0.08	0.05	8.88	-0.01	97.46	2.248	1.504	1.248	0.010	0.006	3.974	0.75
FIM21	D	$2H_2$+$2H_1$	40.12	29.71	18.64	0.07	0.06	8.88	-0.01	97.47	2.250	1.499	1.250	0.009	0.007	3.975	0.75
mean			39.55	30.48	18.23	0.08	0.06	8.84	-0.01	97.22	2.228	1.545	1.228	0.010	0.007	3.973	0.77
FIM28	A	$3T$	39.52	31.50	18.08	0.05	0.04	8.94	-0.01	98.12	2.208	1.584	1.208	0.007	0.005	3.982	0.79
FIM28	A	$3T$	39.10	32.61	17.71	0.04	0.00	8.97	0.00	98.43	2.181	1.637	1.181	0.005	0.000	3.991	0.82
FIM28	A	$3T$	38.99	33.09	17.59	0.06	0.04	8.96	-0.01	98.73	2.171	1.658	1.171	0.007	0.005	3.980	0.83
FIM28	A	$3T$	38.92	32.90	17.57	0.04	0.00	8.96	0.00	98.39	2.173	1.653	1.173	0.006	0.000	3.989	0.83
FIM28	A	$3T$	39.13	32.43	17.75	0.03	0.04	8.95	-0.01	98.33	2.185	1.630	1.185	0.004	0.005	3.987	0.81
FIM28	A	$3T$	38.68	32.67	17.47	0.04	0.04	8.89	-0.01	97.79	2.174	1.652	1.174	0.006	0.005	3.984	0.83
mean			39.06	32.54	17.70	0.04	0.03	8.94	-0.01	98.30	2.182	1.636	1.182	0.006	0.003	3.986	0.82

Chemical composition

In BSE images, all studied cronstedtite crystals from both localities have uniform brightness which indicates their compositional homogeneity (Fig. 6). Despite the topographical and geological differences of both localities, chemical compositions of studied cronstedtite samples are similar (Fig. 7).

On the basis of chemical composition (Tables 3 and 4) it is possible to maintain that polytypes of OD subfamilies (Bailey's groups) A (3*T*) from both localities are relatively Fe-rich (x in the range 0.79 - 0.83) whereas those belonging to D ($2H_2$-$2H_1$) are Fe-poor (0.74 - 0.83). Besides the major Si and Fe contents, small amounts of S (up to 0.02 *apfu*) were detected in all samples (Fig. 7). A similar sulphur contents are known only from cronstedtite from Nižná Slaná (Hybler et al. 2017) and some cronstedtites of meteoritic origin, *e.g*. from the Murchison (Fuchs et al. 1973), Cochabamba (Müller et al. 1979), and Cold Bokkeveld CM chondrites (Tomeoka and Buseck 1985). Sulphur only rarely enters layered silicates; the well-known example is rare brittle mica anandite (Pattiaratchi et al. 1967; Giuseppetti and Tadini 1972; Filut et al. 1985; Bujnowski et al. 2009). In anandite, however, S fully occupies one distinct position, while in cronstedtite only partial substitution of S for OH is assumed (Hybler et al. 2017). The minor contents of Cl (up to 0.01 *apfu*) were also determined in samples from Francisco I. Madero mine (FIM), on the contrary to cronstedtite from San Antonio mine (MSA) which is Cl-free. The presence of minor Cl in cronstedtite is already known, e. g. from Pohled (Hybler et al. 2016), Chyňava (Hybler and Sejkora 2017), Nižná Slaná (Hybler et al. 2017), Litošice (Hybler et al. 2021b) or Ouedi Beht (Hybler et al. 2021a).

Conclusion

This study represents a further example of identification of cronstedtite polytypes using pre-experiments on diffractometers with area detectors and appropriate software. Cronstedtite from two Mexican localities - San Antonio mine, Chihuahua (MSA) and Francisco I. Madero mine (FIM), Zacatecas were studied. The reciprocal space sections were generated by the diffractometer software in order to determine OD subfamilies (Bailey's groups), and particular polytypes. In the samples from MSA the polytype 3*T* (Subfamily A) is the most frequent. Some crystals are affected by twinning by reticular merohedry with the 180° rotation as twinning operation (obverse-reverse twinning). The $2H_2$ polytype (subfamily D) occurs rarely. In the FIM sample, the $2H_1$ + $2H_2$ allotwins (subfamily D) are the most frequent. In one sample, the rare $6T_1$ polytype (subfamily D) was detected. The 3*T* polytype is rare. Besides minor content of Cl in cronstedtite from Francisco I. Madero Mine, the unusual small amounts of sulphur in samples from both studied localities were recorded.

Acknowledgements

This study was financially supported by the Ministry of Culture of the Czech Republic (long-term project DKRVO 2024-2028/1.II.a; National Museum, 00023272).

References

Bailey SW (1969) Polytypism of trioctahedral 1:1 layer silicates. Clays Clay Miner 17: 355-371

Bailey SW (1988) Polytypism of 1:1 layer silicates. Rev Mineral 19: 1-27

Bujnowski TJ, Guggenheim S, Kato T (2009) Crystal structure determination of anandite-2M mica. Am Mineral 94: 1144-1152

Camprubí A, González-Partida E, Torró L, Alfonso P, Canet C, Miranda-Gasca MA, Martini M, González-Sánchez F (2017) Mesozoic volcanogenic massive sulfide (VMS) deposits in Mexico. Ore Geol Rev 81(3): 1066-1083

Canet C, Camprubí A, González-Partida E, Linares C, Alfonso P, Piñeiro-Fernández, F, Prol-Ledesma RM (2009a) Mineral assemblages of the Francisco I. Madero Zn-Cu-Pb-(Ag) deposit, Zacatecas, Mexico: Implications for ore deposit genesis. Ore Geol Rev 35(3-4): 423-435

Canet C, Camprubí A, González-Partida E, Linares C, Alfonso P, Piñeiro-Fernández F, Prol-Ledesma RM (2009b) The Francisco I. Madero Zn-Cu-Pb-(Ag) deposit, Zacatecas, Mexico: Mineral chemistry and fluid inclusion data. J Geochem Explor 101(1): 20

Dornberger-Schiff K, Ďurovič S (1975a) OD-interpretation of kaolinite-type structure - I: symmetry of kaolinite packets and their stacking possibilities. Clays Clay Miner 23: 219-229

Dornberger-Schiff K, Ďurovič S (1975b) OD-interpretation of kaolinite-type structures - II: the regular polytypes (MDO-polytypes) and their derivation. Clays Clay Miner 23: 231-246

Ďurovič S (1981) OD-Charakter, Polytypie und Identifikation von Schichtsilikaten. Fortsch Mineral 59: 191-226

Ďurovič S (1997) Cronstedtite-1M and coexistence of 1M and 3T polytypes. Ceramics-Silikáty 41: 98-104

Filut MA, Rule AC, Bailey SW (1985) Crystal structure refinement of anandite-2Or, a barium and sulphur-bearing trioctahedral mica. Am Mineral 70: 1298-1308

Frondel C (1962) Polytypism in cronstedtite. Am Mineral 47: 781-783

Fuchs LH, Olsen E, Jensen KJ (1973) Mineralogy, mineral-chemistry, and ccomposition of the Murchison (CM) meteorite. Smithson Contrib Earth Sci 10: 1-39

Garvie LA (2021) Mineralogy of the 2019 Aguas Zarcas (CM2) carbonaceous chondrite meteorite fall. Am Mineral 106(12): 1900-1916

Giuseppetti G, Tadini C (1972) The crystal structure of 2O brittle mica: Anandite. Tscherm Min Petrol Mitt 18: 169-184

Hall SH, Guggenheim S, Moore P, Bailey SW (1976) The structure of Unst-type 6-layer serpentines. Can Mineral 14: 314-321

Hybler J, Sejkora J (2017) Polytypism of cronstedtite from Chyňava, Czech Republic. J Geosci 62: 137-146

Hybler J, Sejkora J, Venclík V (2016) Polytypism of cronstedtite from Pohled, Czech Republic. Eur J Mineral 28: 765-775

Hybler J, Števko M, Sejkora J (2017) Polytypism of cronstedtite from Nižná Slaná, Slovakia. Eur J Mineral 29: 91-99

Hybler J, Klementová M, Jarošová M, Pignatelli I, Mosser-Ruck R, Ďurovič S (2018) Polytypes identification in trioctahedral layer silicates by electron diffraction and application to cronstedtite mineral synthetized by iron-clay interaction. Clays Clay Mineral 66: 379-402

Hybler J, Dolníček Z, Sejkora J, Števko M (2020) Polytypism of cronstedtite from Nagybörzsöny, Hungary. Clays Clay Mineral 68: 632-645

Hybler J, Dolníček Z, Sejkora J (2021a) Polytypism of cronstedtite from Litošice, Czech Republic. J Geosci 66: 227-242

Hybler J, Dolníček Z, Sejkora J, Števko M (2021b) Polytypism of cronstedtite from Ouedi Beht, El Hammam, Morocco. Clays Clay Mineral 69: 702-734

Pouchou JL, Pichoir F (1985) "PAP" (φρZ) procedure for improved quantitative microanalysis. In: Microbeam Analysis (Armstrong JT, ed.). San Francisco Press, San Francisco: 104-106

Megaw PKM (2018) The Santa Eulalia mining district, Chihuahua, Mexico. Mineral Record 49(1): 4-184

Megaw PKM, Ruiz J, Titley S (1988) High-temperature, carbonate-hosted Ag-Pb-Zn(Cu) deposits of Northern Mexico. Econ Geol 83(8): 1856-1885

Mikloš D (1975) Symmetry and polytypism of trioctahedral kaolin-type minerals. MS, Ph.D. thesis. Institute of Inorganic Chemistry, Slovak Academy of Sciences, Bratislava, Slovakia 144 pp. (in Slovak).

Müller WF, Kurat G, Kracher A (1979) Chemical and crystallographical study of cronstedtite in the matrix of the Cochabamba (CM2) carbonaceous chondrite. Tscherm Min Petrol Mitt 26: 293-304

Pattiaratchi DB, Saari E, Sahama TG (1967) Anandite, a new barium iron silicate from Wilagedera, North Western Province, Ceylon. Mineral Mag 36: 1-4

Pignatelli I, Mugnaioli E, Hybler J, Mosser-Ruck R, Cathelineau M, Michau N (2013) A multi-technique characterisation of cronstedtite synthetized by iron-clay interaction in a step by step cooling procedure. Clays Clay Miner 61: 277-289

Pignatelli I, Mugnaioli E, Marrocchi Y (2018) Cronstedtite polytypes in the Paris meteorite. Eur J Mineral 30(2): 349-354

Pignatelli I, Mosser-Ruck R, Mugnaioli E, Sterpenich J, Gemmi M (2020) The effect of the starting mineralogical mixture on the nature of Fe serpentines obtained during hydrothermal syntheses at 90°C. Clays Clay Miner 68: 394-412

Pouchou J, Pichoir F (1985) „PAP" (φρz) procedure for improved quantitative microanalysis. In: Armstrong JT (ed): Microbeam Analysis: 104-106. San Francisco Press. San Francisco

Rigaku Oxford Diffraction (2021) CrysAlisPro version 171.41.93a, Data collection and data reduction. GUI

Roche MJ, Fox-Powell MG, Hamp RE, Byrne JM (2023) Iron reduction as a viable metabolic pathway in Enceladus' ocean. Int J Astrobiol 22(5): 539-558

Steadman R (1964) The structure of trioctahedral kaolin--type silicates. Acta Cryst 17: 924-927

Steadman R, Nuttall PM (1963) Polymorphism in cronstedtite. Acta Cryst 16: 1-8

Steadman R, Nuttall PM (1964) Further polymorphism in cronstedtite. Acta Cryst 17: 404-406

Steinmann JJ (1820) Chemische Untersuchung des Cronstedtit's, eines neuen Fossils von Příbram in Böhmen. Gottlieb Haase, Prague, 47 pp.

Steinmann JJ (1821) Chemische Untersuchung des Cronstedtit's, eines neuen Fossils von Příbram in Böhmen. J Chem Phys 32: 69-100

Tomeoka K, Buseck PR (1985) Indicators of aqueous alteration in CM carbonaceous chondrites: Microtextures of a layered mineral containing Fe, S, O and Ni. Geochim Cosmochim Acta 49(10): 2149-2163

Vrba K (1886) Vorläufige Notiz über den Cronstedtit von Kuttenberg. Sitzungsberichte der Königlichen Böhmischen Gesselschaft der Wissenschaften 3: 13-19

Weiss Z, Kužvart M (2005) Clay minerals, their nanostructure and use. 1-281. Charles University, Karolinum publishing house, Prague (in Czech).

Zega TJ, Garvie LA, Buseck PR (2003) Nanometer--scale measurements of iron oxidation states of cronstedtite from primitive meteorites. Am Mineral 88(7): 1169-1172

Zolotov MY (2014) Formation of brucite and cronstedtite-bearing mineral assemblages on Ceres. Icarus 228: 13-26

Zolotov MY, Mironenko MV (2013) On the formation of brucite and cronstedtite on Ceres. Meteorit Planet Sci Suppl 76: 5345